Journal of Environmental Chemical Engineering 13 (2025) 119797

Contents lists available at ScienceDirect

Journal of Environmental Chemical Engineering

journal homepage: www.elsevier.com/locate/jece

Per- and polyfluoroalkyl substances (PFAS) removal by microalgae-derived biochar: Valorising from spent biomass after lipid extraction

Duong T. Nguyen [a], Md Abu Hasan Johir [a], Van-Tung Tra [b], Xiaolei Zhang [c], Qiang Liu [c], A.S. Silitonga [a], Brett D. Turner [a], Long D. Nghiem [a,d,*]

[a] Center for Technology in Water and Wastewater, School of Civil and Environmental Engineering, University of Technology Sydney, NSW 2007, Australia
[b] Institute of Applied Technology and Sustainable Development, Nguyen Tat Thanh University, Ho Chi Minh 70000, Viet Nam
[c] School of Environmental & Chemical Engineering, Shanghai University, No. 99 Shangda Road, Shanghai 200444, China
[d] Smart Green Transformation Center, VinUniversity, Hanoi, Viet Nam

ARTICLE INFO

Keywords:
Perfluorooctanoic acid (PFOA)
Perfluorooctanesulfonate (PFOS)
Adsorption
Biochar
Scenedesmus sp.
Chlorella vulgaris

ABSTRACT

Per- and polyfluoroalkyl substances (PFAS) are persistent environmental contaminants of concern due to their toxicity and resistance to conventional water treatment. This study investigates the removal of perfluorooctanoic acid (PFOA) and perfluorooctanesulfonic acid (PFOS) – two most prominent PFAS compounds, using biochar derived from microalgae spent biomass. Biochars derived from *C. vulgaris* and *Scenedesmus* sp. biomass were evaluated for PFAS adsorption. Compared to granular activated carbon (GAC), biochars showed faster kinetics, reaching equilibrium within 2 h. *Scenedesmus* sp. biochar exhibited higher adsorption capacities (30.1 μg/g PFOA; 43.1 μg/g PFOS) than *C. vulgaris* biochar and, at 0.25 g/L of biochar, both biochars completely removed PFAS in single-solute systems. Under natural organic matter competition, *Scenedesmus* sp. biochar maintained > 80 % PFOA and 87 % PFOS removal at 1 g/L of biochar. Adsorption was dominated by hydrophobic interactions with secondary cation bridging. While capacities were lower than GAC, microalgal biomass represents a sustainable feedstock to produce biochars for PFAS adsorption. The results demonstrate that the developed biochar exhibits rapid uptake of PFAS, highlighting its potential as an effective and sustainable material for water treatment applications.

1. Introduction

Per- and polyfluoroalkyl substances (PFAS), commonly known as "forever chemicals", are fluorine-based compounds first manufactured in the 1940s. PFAS molecules consist of a carbon chain (4–12 carbons) bonded to multiple fluorine atoms, resulting in a compact, dense, and highly hydrophobic structure. Carbon–fluorine (C–F) is one of the strongest bonds in organic chemistry [1]. As such, PFAS are extremely resistant to thermal, chemical, and biological degradation. These properties had led to widespread global usage of PFAS until recently, especially as firefighting foam and even waterproof lining for food packaging. As a result, PFAS are now ubiquitous in the environment, raising concerns about their potential effects on human health and the ecosystem. PFAS occurrences in soil, reclaimed water reservoirs, underground water, and even reservoirs intended for drinking water production have been frequently reported in the literature. The high persistence and bioaccumulation of PFAS have also been well-documented with notable potential epidemiological consequences.

Several methods have been developed to remove PFAS from the aqueous phase, including membrane filtration (nanofiltration or reverse osmosis) [2], advanced oxidation process [3], bioremediation [4], and adsorption [5]. To date, given the scale of water resource contamination, adsorption has probably been the most widely applied technique for PFAS removal due to flexibility, scalability, cost-effectiveness, and high removal efficiency [6,7]. A wide range of adsorbents has been developed, evaluated, and applied at an industrial scale for PFAS removal [8]. Granular activated carbon (GAC) and anion-exchange resins are the two most mature adsorbents for PFAS removal [9]. Biochar has also emerged as a low-cost adsorbent for PFAS removal due to its multiple physicochemical mechanisms. Removal is mainly driven by hydrophobic interactions between the fluorinated tails and biochar's nonpolar surfaces, with additional contributions from electrostatic

* Corresponding author at: Center for Technology in Water and Wastewater, School of Civil and Environmental Engineering, University of Technology Sydney, NSW 2007, Australia.
E-mail address: Duclong.nghiem@uts.edu.au (L.D. Nghiem).

https://doi.org/10.1016/j.jece.2025.119797
Received 1 September 2025; Received in revised form 5 October 2025; Accepted 13 October 2025
Available online 13 October 2025

interactions, pore entrapment, and hydrogen bonding via surface functional groups [10-12]. Overall, PFAS adsorption efficiency is governed by biochar's surface properties and the solution chemistry.

Biochar derived from agricultural wastes such as straw and sawdust has been demonstrated to be highly effective for PFAS removal [10,13]. In contrast, the use of microalgae, particularly their spent biomass, remains largely unexplored as a feedstock for biochar production and PFAS removal applications. The development of the microalgae-based biofuel industry results in substantial amounts of microalgal biomass waste. It is estimated that the oil extraction step in biodiesel production can generate up to 70 % biomass residue by mass [14]. Following extraction, the waste biomass can be converted into biochar, which enhances the process of producing biofuel and encourages the use of circular economy principles. Although agricultural waste is inexpensive and accessible, microalgal biomass offers scalability benefits due to its capacity to be continually grown and connected to wastewater treatment. Using discarded biomass from the biofuel sectors could offset costs and position microalgae-derived biochar as a competitive and sustainable option, even if producing microalgal biomass is currently more expensive than using agricultural wastes [15]. Biochar derived from microalgae has shown high adsorption efficiency and rapid uptake for various organic pollutants, such as dyes [16], and heavy metals [17], highlighting its potential as a versatile sorbent. Beyond pollutant removal, microalgae biochar contributes to carbon neutrality, providing dual-path valorisation. Microalgae offer a sustainable feedstock due to their fast growth, high CO_2 absorption, and minimal land requirements, as they do not compete with arable land, making them more environmentally favorable than conventional plant-based adsorbents. This makes a substantial contribution to improving environmental sustainability and lowering carbon footprints.

Because microalgae-derived biochar is porous and hydrophobic, it may effectively adsorb hydrophobic organic pollutants like PFAS. However, no prior research has looked into the adsorption of PFAS using biochar made from wasted microalgae biomass. To fill the aforementioned gap, this study compares the effectiveness of two types of biochar made from the spent biomass of *C. vulgaris* and *Scenedesmus* sp. species with commercial GAC in terms of removing the two most well-known PFAS compounds, perfluorooctanoic acid (PFOA) and perfluorooctanesulfonic acid (PFOS). This study evaluates the adsorption performance and mechanisms of microalgae-derived biochar by examining kinetics, equilibrium isotherms, pH effects, and competitive adsorption with natural organic matter (NOM). The work aims to clarify the factors controlling PFAS removal and demonstrate the potential of microalgae-based biochar as a sustainable, high-performance adsorbent for the removal of emerging contaminants.

2. Materials and methods

2.1. Microalgae-derived biochar

Spent biomass from *C. vulgaris* and *Scenedesmus* sp. was obtained after Soxhlet lipid extraction with n-hexane, washed, oven-dried (60 °C, 24 h), ground, and sieved (150 μm). Biochar was produced via pyrolysis at 600 °C for 2 h under N_2 (1 L/min, 10 °C/min), yielding 35 % of the final product. High-temperature pyrolysis enhanced carbonization, hydrophobicity, and porosity [18]. The resulting biochar was washed, dried, and used for PFAS adsorption experiments.

2.2. Granular activated carbon

Commercial granular activated carbon (GAC, AquaSorb® HS, Jacobi Carbons), derived from coconut shells and steam-activated, was used at the same solid-to-liquid ratio as microalgae biochar to benchmark PFAS removal. Comparing biochar with an industry-standard adsorbent provides a reference for evaluating adsorption efficiency and assessing the practical potential of microalgae-derived biochar as a sustainable alternative.

2.3. Microalgae-derived biochar and GAC characterization

Biochars and GAC were characterized for surface area, functional groups, morphology, elemental composition, and surface charge. Specific surface area via nitrogen adsorption was determined based on Brunauer–Emmett–Teller (BET) analysis (Quantachrome Autosorb-iQ3-MP/Kr). Surface functional groups were identified using FTIR (Shimadzu MIRacle 10, 4000–450 cm^{-1}). Morphology and elemental composition were assessed using SEM-EDS (Zeiss Supra 55VP with Oxford Instruments), with samples sputter-coated in chromium. Zeta potential was measured at varying pH (0.025 g adsorbent in 100 mL 1 mM KCl, pre-equilibrated 24 h) using a Malvern Zetasizer Ultra, with triplicate measurements and 30 scans per sample.

2.4. Chemicals and reagents

PFOA and PFOS standards were obtained from Sigma-Aldrich (Australia). LCMS-grade methanol, ammonium acetate, humic acid, NaOH, and H_2SO_4 were of analytical grade and used as received.

2.5. Analytical methods

PFAS concentrations were measured using a Shimadzu LCMS-8060 triple quadrupole MS (Shimadzu, Japan) with a Kinetex EVO C18 column (100 ×2.1 mm, 5 μmm), employing negative-mode electrospray ionisation (ESI) and multiple reaction monitoring (MRM) for quantification. A calibration curve was made using standards ranging from 0.02 to 20 μg/L. Samples were filtered (0.2 μm RC) before analysis. Control analyses confirmed the absence of PFAS contamination or loss. Moreover, to minimize matrix effects, chromatographic separation was optimized on a Kinetex EVO C18 column using a methanol–water gradient with 5 mM ammonium acetate as a volatile buffer, which ensured a stable signal while avoiding non-volatile residue accumulation in the ion source. Matrix blanks and control/initial samples of the matrix were included in each batch to monitor background interference and to calculate sorption capacity or removal efficiency. These measures collectively minimized the influence of NOM and other substances on LC-MS/MS detection of PFOA and PFOS. Supplementary Tables S1 and S2 provide detailed LC-MS conditions and MRM parameters. Total dissolved organic carbon (DOC) in humic acid–based natural organic matter (NOM) matrices was measured using a Multi N/C TOC analyzer after filtering using 1.2 μm, and pH was recorded with a HACH HQ40d MultiMeter.

2.6. Adsorption experiments

2.6.1. Batch adsorption setup

PFAS adsorption experiments were conducted in polypropylene containers at 20 ± 2 °C with shaking at 200 rpm. Single-solute tests used 100 mL solutions of PFOA or PFOS (4 μg/L) with 0.25 g/L adsorbent, while competitive experiments included both PFAS (4 μg/L each) and humic acid (5 mg/L DOC) at adsorbent dosages of 0.5–1 g/L. The chosen concentration, 4 μg/L, is within the median range reported for groundwater and surface water [19]. This elevated concentration was to ensure high throughput and accurate PFAS analysis. It also presents a challenging condition and to assess the adsorption capacity of the biochar under relatively high PFAS levels that may occur in industrial effluents or heavily contaminated sites. All experiments were performed in duplicate with controls. Samples were collected at predetermined intervals, filtered (0.2 μm RC), and analyzed, with controls confirming no PFAS contamination from containers or filters.

The removal efficiency of each PFAS was calculated using Eq. 1:

$$R\ (\%) = \frac{(C_0 - C_e) \times 100}{C_0} \quad (1)$$

Where R (%) is the removal efficiency, C_0 (μg/L) is the initial PFAS concentration, and C_e (μg/L) is the equilibrium PFAS concentration.

2.6.2. Adsorption kinetics

PFAS adsorption kinetics were assessed by sampling at specific times up to 120 min for biochar and 480 min for GAC. Data were fitted using pseudo-first-order and pseudo-second-order kinetic models [20] to evaluate adsorption rates as described in Eq. 2 and Eq. 3, respectively.

$$q_t = q_e(1 - e^{-k_1 t}) \quad (2)$$

$$q_t = \frac{k_2 q_e^2 t}{1 + k_2 q_e t} \quad (3)$$

Where t (min) is the contact time; q_t (μg/g) is the PFAS uptake per unit mass of adsorbent at time *t*; q_e (μg/g) is the q_t value at equilibrium state; k_1 (min^{-1}) and k_2 (g/μg.min) are the pseudo-first-order and pseudo-second-order model constants, respectively. The kinetic parameters (q_e, k_1, and k_2) were determined by fitting experimental data to pseudo-first-order and pseudo-second-order kinetic models using non-linear regression.

The amount of PFAS adsorbed per unit mass of adsorbent at time t was calculated using Eq. 4:

$$q_t = \frac{(C_0 - C_t)V}{m} \quad (4)$$

Where q_t (μg/g) is the mass of PFAS adsorbed per unit mass of adsorbents; C_0 (μg/L) is the initial concentration of PFAS in the solution; C_t (μg/L) is the concentration of PFAS in the supernatant at time t; V (L) is the solution volume; and m (g) is the amount of adsorbent.

2.6.3. Equilibrium adsorption isotherms

Batch adsorption isotherms were conducted using PFOA or PFOS solutions (0.5–20 μg/L) with 0.25 g/L adsorbent, shaken at 200 rpm for 24 h to reach equilibrium. Data were fitted to Langmuir (Eq. 5) [21] and Freundlich (Eq. 6) [22] isotherm models to determine adsorption capacities.

$$q_e = \frac{K_L q_{max} C_e}{1 + K_L C_e} \quad (5)$$

$$q_e = K_F C_e^{1/n} \quad (6)$$

Where q_e (μg/g) and C_e (μg/L) are the equilibrium concentration of PFAS in the solid (adsorbent) and aqueous phase, respectively; K_L (L/μg) is the Langmuir adsorption constant; K_F (μg/g)/(μg/L)$^{1/n}$ is the Freundlich adsorption constant; n represents adsorption intensity; q_{max} is the adsorption capacity of the adsorbent (μg/g). The adsorption isotherm parameter (K_L, K_F, n, and q_{max}) were determined by the experimental equilibrium data to the Langmuir and Freundlich models using non-linear regression.

2.6.4. Effect of pH

The effect of pH on PFOA and PFOS adsorption was evaluated over pH 4–10. The solution pH was adjusted using 0.1 M HCl or 0.1 M NaOH solution. Solutions (100 mL, 4 μg/L) with 0.25 g/L adsorbent were shaken at 200 rpm for 24 h to reach equilibrium. Final pH was measured to assess potential adsorption-related changes in solution chemistry or adsorbent surface charge.

2.6.5. Competitive adsorption

Natural waters and wastewater typically contain mixtures of PFAS alongside NOM. Thus, batch competitive adsorption experiments were conducted to assess PFAS removal in the presence of NOM, simulated with humic acid (5 mg/L DOC). PFOA and PFOS of 4 μg/L each were used in the test solution. Experimental procedures, sampling, and analysis followed the same protocol as the isotherm studies to evaluate competitive effects on adsorption performance.

Table 1
Specific surface area and zeta potential of microalgae-derived biochar and GAC.

Adsorbents	BET surface area (m^2/g)	Zeta potential (mV) (at pH=7)
C. vulgaris biochar	23	−22.4
Scenedesmus sp. biochar	37	−38.7
GAC	1050	−23.2

3. Results and discussions

3.1. Microalgae-derived biochar and GAC characterisation

Surface properties of biochars, and GAC were characterized using BET surface area, zeta potential, FTIR spectroscopy, SEM, and EDS to elucidate mechanisms governing PFAS interactions.

PFAS adsorption correlated with adsorbent surface area, as larger surface areas provide more active sites [6]. GAC showed the highest specific surface area, while among the microalgae biochars, *Scenedesmus* sp. biochar had a higher surface area than *C. vulgaris* biochar (Table 1). Although biochars had lower surface areas than GAC, SEM imaging (Supplementary Data, Fig. S4) revealed porous micro- and meso-structures conducive to PFAS adsorption. Additionally, *Scenedesmus* sp. biochar exhibited a more developed porosity, indicating greater adsorption potential.

Zeta potential analysis revealed that both microalgae-derived biochar and GAC possess negative surface charges at neutral pH (Table 1), which become increasingly negative with increasing pH (Supplementary Data, Fig. S6). This behavior is primarily due to the deprotonation of oxygen-containing surface functional groups [23], such as hydroxyl (O–H) and ether-like (C–O) moieties, as confirmed by FTIR analysis (Supplementary Data, Fig. S5). At low pH, these groups remain partially protonated, resulting in less negative surface charges, whereas higher pH promotes deprotonation (e.g., $–O^-$), enhancing negative surface potential [24]. This pH-dependent charge behavior, characteristic of carbonaceous adsorbents, directly affects interactions with anionic PFAS: electrostatic repulsion increases at higher pH, potentially reducing adsorption efficiency for negatively charged contaminants [25].

FTIR spectra of *C. vulgaris* and *Scenedesmus* sp. biochars exhibited characteristic peaks near 1600 cm^{-1} and 2900 cm^{-1} , corresponding to aromatic C=C and aliphatic C–H stretching, respectively (Supplementary Data, Fig. S5), indicating graphitic and hydrophobic domains on the carbon surface [26]. These structural features reinforce the non-polar, aromatic nature of microalgae-derived biochar and its low water affinity, which favor adsorption of hydrophobic PFAS moieties. Elemental analysis (EDS) revealed inorganic constituents, including magnesium and calcium, originating from the microalgal biomass (Supplementary Data, Fig. S4). These mineral cations can act as bridging agents, linking negatively charged PFAS headgroups to the similarly charged biochar surface, thereby mitigating electrostatic repulsion and enhancing adsorption [27]. Collectively, the combination of hydrophobic/aromatic domains and surface minerals underpins the dual-mode adsorption mechanisms of microalgae-derived biochars.

3.2. Adsorption kinetics

The adsorption kinetics of PFOA and PFOS revealed rapid uptake by microalgae-derived biochars, reaching apparent equilibrium within 2 h. *Scenedesmus* sp. biochar demonstrated particularly fast and efficient removal, achieving 99 % PFOA removal within 60 min. In contrast, GAC

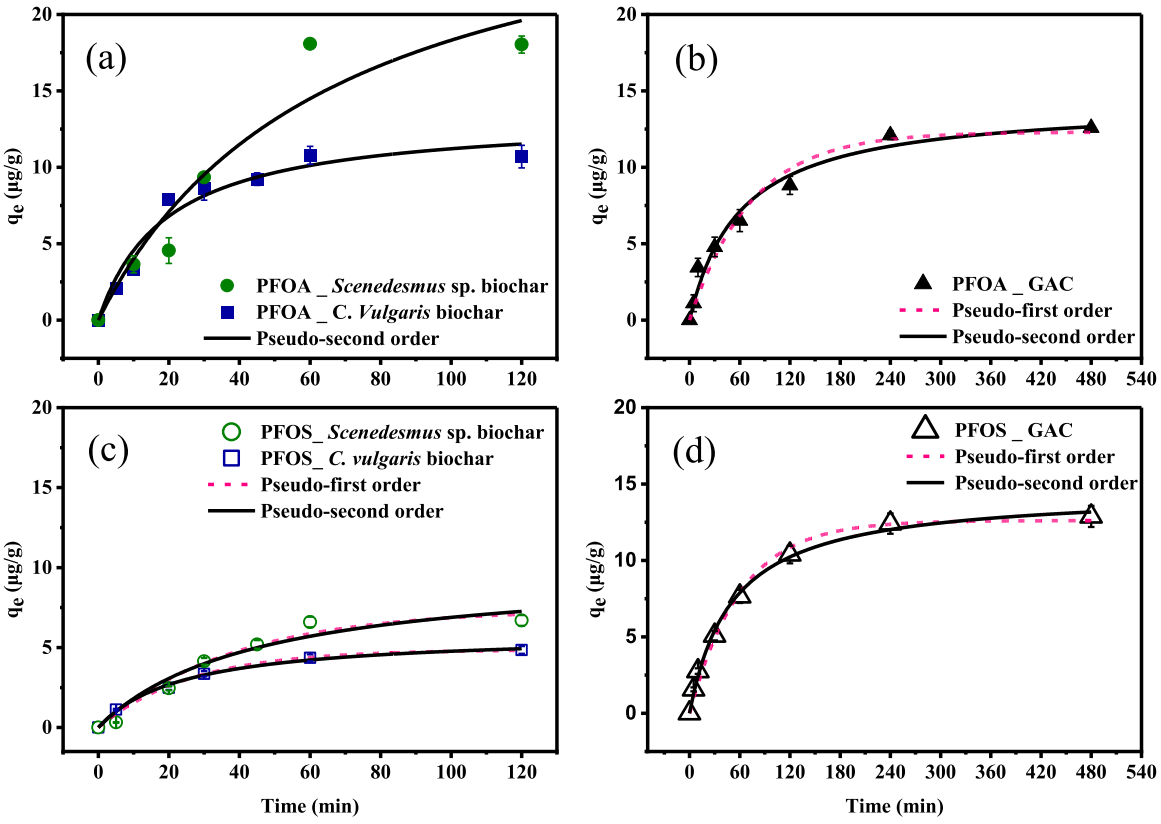

Fig. 1. Kinetic model fitting for PFAS adsorption onto microalgae-derived biochar and GAC: PFOA adsorption (a) and (b); PFOS adsorption (c) and (d). Experimental conditions: initial PFOA or PFOS concentration = 4 µg/L, adsorbent dosage = 0.25 g/L, pH = 6.5 for PFOA and 6.0 for PFOS, temperature = 20 ± 2 °C. Error bars present the standard deviation of two replicating experiments.

Table 2
Kinetic parameters calculated from the pseudo-first-order and pseudo-second-order models for the single-solute adsorption of PFOA and PFOS onto biochar and GAC. (Experimental conditions: initial PFOA or PFOS concentration = 4 µg/L, adsorbent dosage = 0.25 g/L, pH = 6.5 for PFOA and 6.0 for PFOS, temperature = 20 ± 2 °C.).

Adsorbents	Pseudo-first order model			Pseudo-second order model		
	q_e (µg/g)	K_1 (min^{-1})	R^2	q_e (µg/g)	K_2 (g/µg.min)	R^2
	PFOA					
C. vulgaris biochar	7.5 ± 1.2	133.5	0.406	13.4 ± 1.1	0.052	0.962
Scenedesmus sp. biochar	10.7 ± 3.1	362.8	0.327	30.9 ± 8.7	0.036	0.913
GAC	12.3 ± 0.8	0.014	0.965	14.2 ± 0.9	0.017	0.979
	PFOS					
C. vulgaris biochar	4.9 ± 0.1	0.038	0.995	5.9 ± 0.2	0.041	0.995
Scenedesmus sp. biochar	7.4 ± 0.7	0.026	0.970	9.9 ± 1.7	0.042	0.996
GAC	12.6 ± 0.4	0.016	0.992	14.6 ± 0.9	0.020	0.996

exhibited slower kinetics, requiring approximately 8 h to reach near-equilibrium with ~97 % removal. These findings align with previous reports indicating that biochar generally exhibits faster PFAS adsorption than GAC, likely due to accessible porosity, surface functional groups, and favorable hydrophobic and electrostatic interactions [28,29].

The adsorption of both PFOA and PFOS was better described by the pseudo-second-order model, with R^2 values of over 0.91 (Fig. 1 and Table 2). In contrast, the pseudo-first-order model provided a poor fit—for instance, R^2 values were below 0.41 for PFOA adsorption onto microalgae biochar.

The poor fit of the pseudo-first-order model indicates that the process is not controlled by simple physical adsorption. This model does not adequately capture the complexity of the interactions involved. Instead, the adsorption process is likely governed by hydrophobic interactions and site-specific adsorption mechanisms, where the availability and accessibility of active sites play a critical role. These characteristics are more accurately represented by the pseudo-second-order model.

It is noteworthy that the pseudo-second-order fitted q_e values for biochars were comparable to, or higher than, those of GAC despite GAC's much larger surface area. This apparent discrepancy arises because PFAS adsorption is controlled more by surface chemistry, pore accessibility, and hydrophobic domains than by the total surface area.

The higher pseudo-second-order rate constants (K_2) observed for biochars (0.036–0.052 g/µg·min) compared to GAC (0.017–0.020 g/µg·min) further confirm the faster adsorption kinetics. Although adsorption is governed by site-specific interactions, the rapid approach to equilibrium is facilitated by the high external surface accessibility of microalgae-derived biochar. In fine powder form, the biochar exhibits shorter diffusion pathways and disperses more effectively in solution, allowing faster contact with PFOA and PFOS molecules. This promotes rapid surface adsorption through hydrophobic interactions.

While GAC has a higher surface area than biochar (Table 1), its larger

Table 3
Isotherm parameters calculated from the Langmuir and Freundlich models for the single-solute adsorption of PFOA and PFOS onto biochar and GAC. Experimental conditions: initial PFOA or PFOS concentration = 0.05–20 μg/L, adsorbent dosage = 0.25 g/L, pH = 6.5 for PFOA and 6.0 for PFOS, temperature = 20 ± 2 °C.

Adsorbents	Langmuir model			Freundlich model		
	q_{max} (μg/g)	K_L (L/μg)	R^2	K_F [(μg/g)(L/μg)$^{1/n}$]	n	R^2
	PFOA					
C. vulgaris biochar	21.4 ± 1.8	0.82	0.932	8.88	3.20	0.832
Scenedesmus sp. biochar	30.1 ± 3.6	0.31	0.949	7.49	2.11	0.872
GAC	79.4 ± 21.4	12.4	0.790	121	1.98	0.727
	PFOS					
C. vulgaris biochar	35.7 ± 5.0	0.10	0.982	4.29	1.61	0.982
Scenedesmus sp. biochar	43.1 ± 7.5	0.14	0.965	6.78	1.76	0.980
GAC	319 ± 273	0.04	0.979	11.9	1.18	0.983

Table 4
Fluorine content (wt%) measured by EDS before and after PFAS adsorption.

Adsorbents	Before adsorption	After adsorption PFOA	After adsorption PFOS
C. vulgaris biochar	ND	0.49	0.62
Scenedesmus sp. biochar	ND	0.62	0.80
GAC	ND	1.12	1.30

Note: ND = not detected.

particle size and highly microporous structure result in slower diffusion and delayed adsorption kinetics. These results highlight the advantage of microalgae-derived biochar for applications where rapid PFAS removal is essential. In practical treatment systems, fast adsorption is particularly important, as it can reduce contact time, lower operational costs, increase system throughput, and allow for more compact reactor designs.

3.3. Adsorption isotherms

Adsorption isotherms were used to evaluate the capacity and mechanisms of PFOA and PFOS removal by microalgae-derived biochars and GAC. GAC exhibited the highest adsorption capacities, with q_{max} values of 79 μg/g for PFOA and 319 μg/g for PFOS (Table 3), reflecting its large surface area and well-developed porous structure. Among the biochars, *Scenedesmus* sp. consistently outperformed *C. vulgaris*, achieving higher q_{max} values for PFOS (43.1 vs. 35.7 μg/g) and PFOA (30.1 vs. 21.4 μg/g) (Table 3). PFOS showed greater adsorption than PFOA across all adsorbents, likely due to its longer carbon chain and higher hydrophobicity. Langmuir and Freundlich models (Fig. 3 and Table 3) were applied to describe adsorption behavior, suggesting monolayer adsorption predominated on GAC, whereas heterogeneous adsorption sites were more relevant for biochars. EDS analysis confirmed PFAS uptake through the detection of fluorine at adsorbent surfaces (Table 4), corroborating quantitative adsorption data and supporting the potential of microalgae biochars as practical PFAS sorbents.

PFOA adsorption onto biochars was better described by the Langmuir model (Table 3), indicating monolayer adsorption on relatively homogeneous active sites. Freundlich isotherms yielded 'n' values greater than unity, reflecting favorable adsorption conditions [30]. The highest Freundlich constant (K_F) values observed for GAC are consistent with its high adsorption capacity, as also indicated by its maximum adsorption capacity (q_{max}) and Langmuir constant (K_L). Notably, the Langmuir K_L values for PFOS adsorption onto biochar were low, likely due to the trace PFAS concentrations used (0.5–20 μg/L), which fall within the linear region of the isotherm and may underestimate the true adsorption affinity. Isotherm data also emphasized the dominant role of hydrophobic interactions: PFOS exhibited higher adsorption than PFOA due to its longer perfluorinated carbon chain and sulfonic acid group ($–SO_3^-$), compared to the carboxylic acid group (–COOH) in PFOA. Despite these differences, microalgae biochars demonstrated appreciable adsorption at environmentally relevant concentrations, supporting their potential as sustainable adsorbents for legacy PFAS.

Scenedesmus sp. derived biochar exhibited higher adsorption capacities for PFOA and PFOS compared to *C. vulgaris*, reflecting its greater specific surface area and structural features. FTIR analysis indicated enhanced aromatic C=C content and the presence of a C–O functional group, which may facilitate weak hydrogen-bonding interactions with PFAS [31]. Due to electrostatic repulsion between the negatively

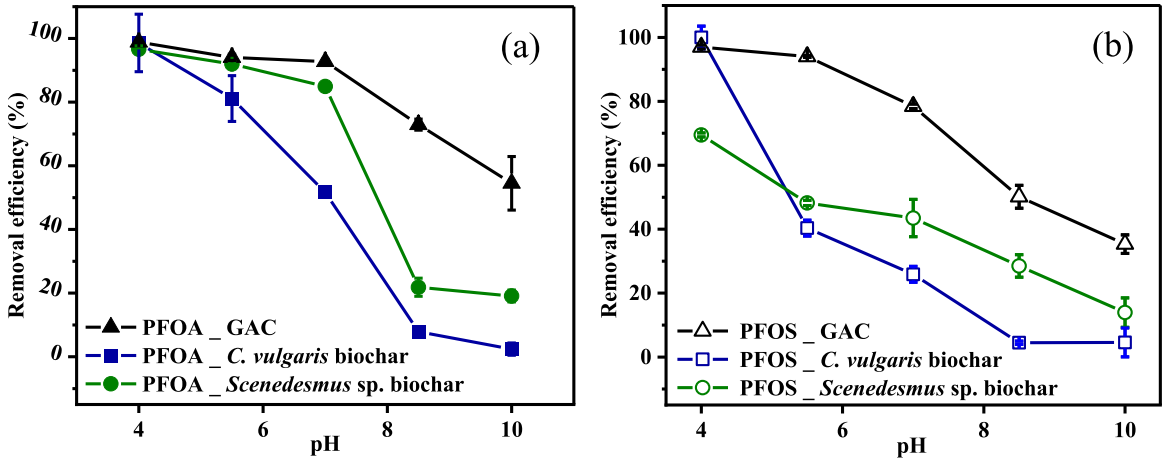

Fig. 2. Effect of pH on the adsorption capacity of PFOA (a) and PFOS (b) in single-solute mode. Experimental conditions: initial pH range = 4–10, PFOA or PFOS concentration = 4 μg/L, adsorbent dosage = 0.25 g/L, temperature = 20 ± 2 °C. Error bars present the standard deviation of two replicating experiments.

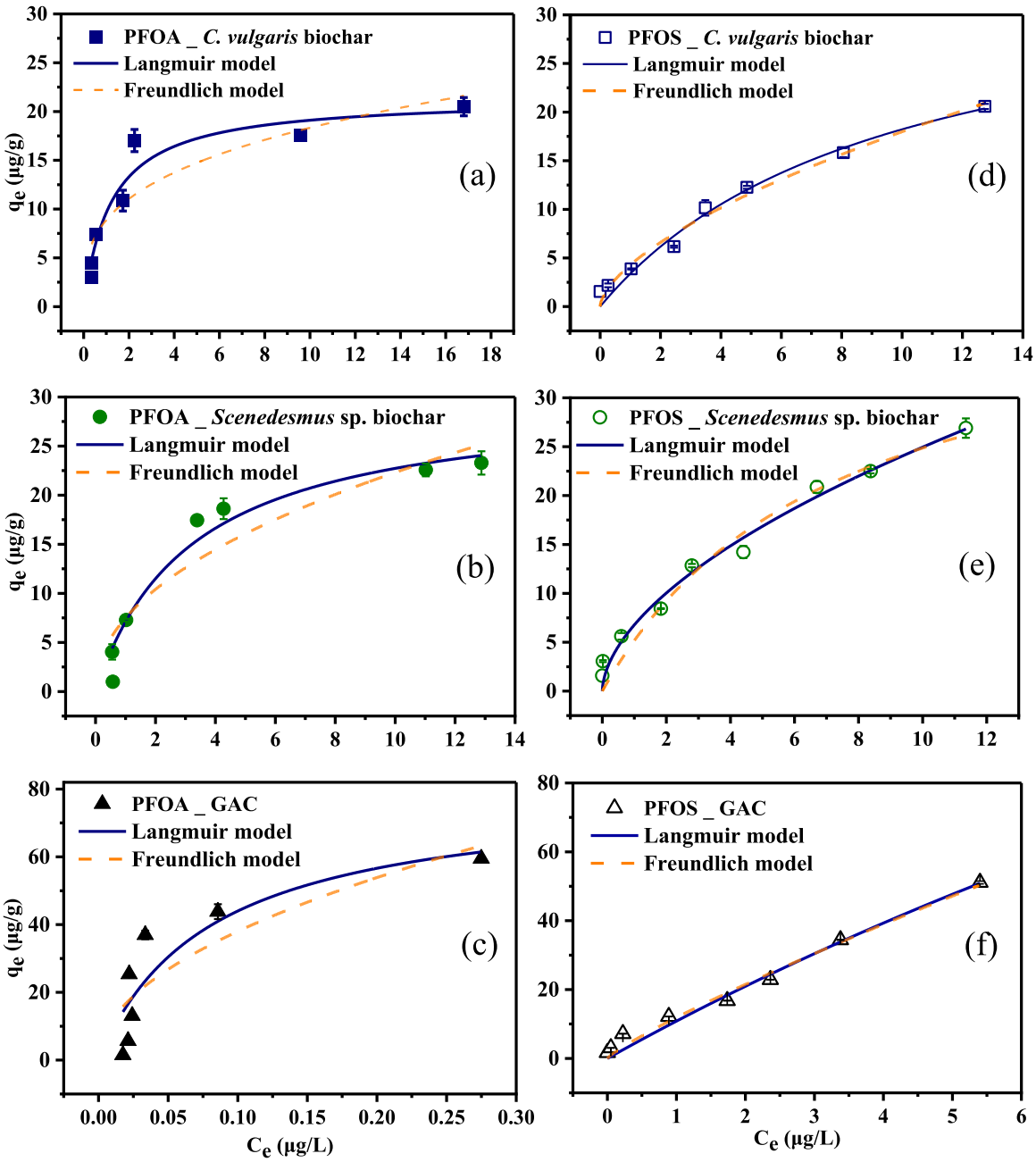

Fig. 3. Isotherm model fitting for PFAS adsorption onto microalgae-derived biochar and GAC: PFOA adsorption (a), (b), and (c); PFOS adsorption (d), (e), and (f). Experimental conditions: initial PFOA or PFOS concentration = 0.05–20 µg/L, adsorbent dosage = 0.25 g/L, pH = 6.5 for PFOA and 6.0 for PFOS, temperature = 20 ± 2 °C. Error bars present the standard deviation of two replicating experiments.

charged PFAS and biochar surfaces, hydrophobic interactions dominate adsorption, with cation bridging providing a secondary mechanism as discussed in Section 3.3. These findings demonstrate that the physicochemical properties of biochars vary by microalgae species, influencing their effectiveness in PFAS removal.

3.4. Effect of pH on single adsorption

The effect of pH on the removal efficiency of PFOA and PFOS by microalgae-derived biochars and GAC is shown in Fig. 2. For both compounds, removal efficiency consistently decreased as pH increased, with this trend being more pronounced for the biochars compared to GAC. In contrast, GAC exhibited a more stable performance across the tested pH range. These results indicate that acidic conditions favor PFAS adsorption, suggesting that pH adjustment may be necessary to optimize the removal efficiency of pristine microalgae biochar.

The acid dissociation constant (pK_a) indicates the pH at which a molecule donates a proton. Both PFOA ($pK_a \approx 2.5–3.8$) and PFOS ($pK_a < 1$) are fully deprotonated and carry a negative charge under all tested pH conditions (pH 4–10) [32]. As pH increases, the adsorbent surface becomes more negatively charged, as confirmed by zeta potential measurements (Fig. S6). This enhances electrostatic repulsion between the negatively charged PFAS molecules and the adsorbent surface, thereby reducing removal efficiency at higher pH values.

Despite the persistent negative surface charge, PFAS were still adsorbed by the biochar, indicating that adsorption is not solely governed by electrostatics. Prior studies have also reported effective PFAS adsorption onto negatively charged carbon-based and mineral surfaces

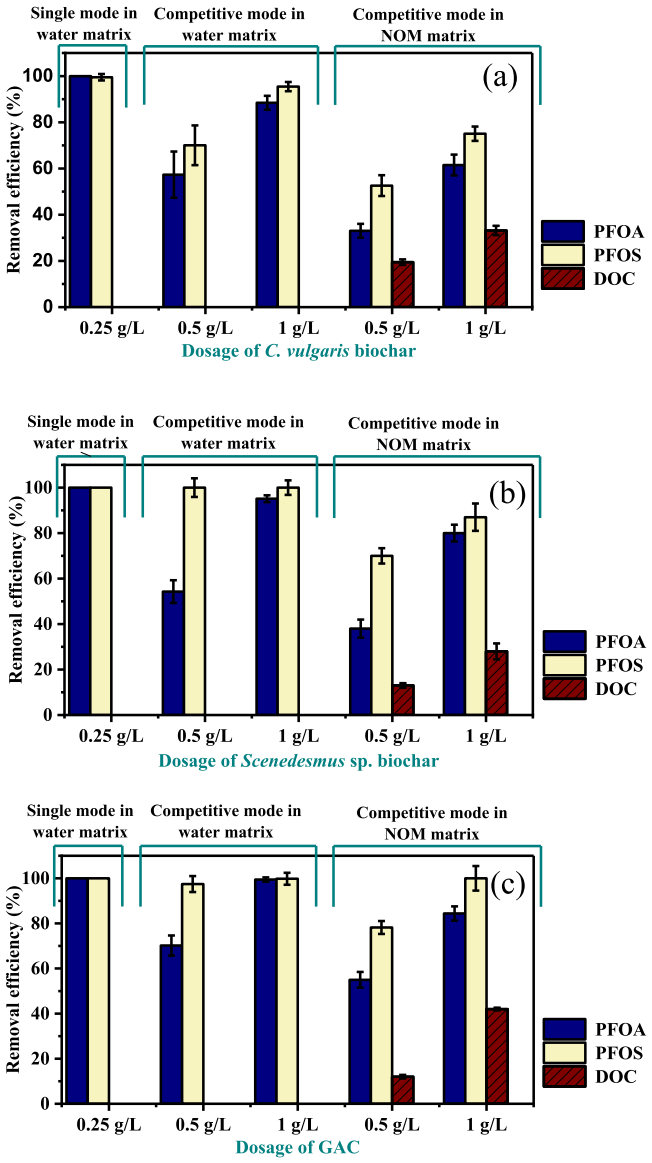

Fig. 4. Removal efficiency of PFOA and PFOS in single and competitive modes using water and NOM matrices for (a) *C. vulgaris* biochar, (b) *Scenedesmus* sp. biochar, and (c) GAC. Experimental conditions: pH = 6.2 ± 0.7, PFOA and PFOS concentration = 4 μg/L, DOC concentration = 5 mg/L, temperature = 20 ± 2 °C. Error bars present the standard deviation of two replicating experiments.

[33,34], supporting the role of non-electrostatic mechanisms. While surface charge is an important factor, it does not fully dictate adsorption performance, particularly in systems where hydrophobic interactions dominate [35]. In such cases, hydrophobic interactions may play a more significant role in overcoming electrostatic repulsion. PFAS, with its highly hydrophobic fluorinated tail, tends to partition into nonpolar regions. Both GAC and biochar, characterized by their hydrophobic surfaces, provide favorable environments for PFAS adsorption through hydrophobic affinity. In this study, the presence of hydrophobic surface domains, evidenced by FTIR peaks corresponding to C–H and C═C bands, likely facilitated the hydrophobic partitioning of PFAS fluorinated tails onto the biochar matrix. This mechanism helps offset electrostatic repulsion, particularly under mildly acidic to neutral pH conditions.

Additionally, elemental analysis revealed that both *C. vulgaris* and *Scenedesmus* sp. biochar contain calcium and magnesium, which may facilitate PFAS adsorption through cation bridging between the negatively charged PFAS headgroups and the biochar surface. This bridging is likely more effective under acidic conditions, where competition from hydroxide ions is minimized. At higher pH, the decline in sorption may therefore be due to both reduced cation bridging efficiency and intensified electrostatic repulsion. The decline is especially evident in *C. vulgaris* biochar, which has a lower surface area and less developed porosity compared to *Scenedesmus* sp. biochar (Table 1 and Fig. S4).

3.5. Competitive adsorption

Competitive adsorption experiments evaluated the removal of PFOA and PFOS by *Scenedesmus* sp. and *C. vulgaris* biochars and GAC in both clean water and in the presence of humic acid as a NOM surrogate. GAC maintained consistent PFAS removal across matrices, while *Scenedesmus* sp. biochar outperformed *C. vulgaris*, particularly under competitive conditions (Fig. 4). In single-solute tests, all adsorbents achieved near-complete removal (100 %) at 0.25 g/L. Under competitive conditions, PFOA removal declined significantly (≈46 % for biochar, 30 % for GAC at 0.5 g/L), whereas PFOS remained largely unaffected (>95 %). The presence of NOM (DOC ≈ 5 mg/L) further reduced adsorption, with PFOS removal dropping to 70 % for *Scenedesmus* sp. biochar and 78 % for GAC; increasing the adsorbent dose to 1 g/L improved removal to 87 % (PFOS) and 80 % (PFOA) (Fig. 4). PFOS consistently showed higher removal due to stronger hydrophobicity. NOM inhibited adsorption by coating surfaces with polar groups, blocking active sites, and reducing hydrophobic interactions, highlighting the influence of matrix complexity on PFAS removal.

3.6. Future outlook

Microalgae-derived biochar shows lower adsorption capacity for PFAS than commercial GAC, with efficiency further reduced by competing organic matter and pH effects. Adsorption can be enhanced through surface activation (e.g., KOH or HCl) and chemical modification (e.g., metal oxide doping or cationic polymer coating) to increase surface area and introduce positively charged sites that mitigate electrostatic repulsion. Combined activation and functionalization is especially promising. Future studies should evaluate performance in complex matrices, such as PFAS mixtures in wastewater or leachate, and assess regenerability over multiple cycles to establish microalgae biochar as a sustainable PFAS remediation option.

4. Conclusions

This study demonstrated microalgae-derived biochar as an effective adsorbent for legacy PFAS, outperforming GAC in adsorption rate and maintaining efficiency in the presence of NOM. Adsorption capacities were species-dependent, with *Scenedesmus* sp. biochar showing superior removal for PFOA (30.1 μg/g) and PFOS (43.1 μg/g). The adsorption process followed Langmuir and the Freundlich models, primarily driven by hydrophobic interactions and assisted by cation bridging. Overall, these results demonstrate the potential to convert waste microalgal biomass from biofuel production into a sustainable material for PFAS remediation.

CRediT authorship contribution statement

A.S. Silitonga: Writing – review & editing, Supervision, Resources. **Qiang Liu:** Writing – review & editing, Visualization, Supervision, Methodology. **Xiaolei Zhang:** Visualization, Resources, Methodology, Data curation. **Van-Tung Tra:** Visualization, Methodology, Investigation. **Brett D. Turner:** Writing – review & editing, Resources, Methodology, Data curation. **Md Abu Hasan Johir:** Writing – review & editing, Resources, Data curation. **Duong T. Nguyen:** Writing – review & editing, Writing – original draft, Methodology, Formal analysis, Data

curation. **Nghiem Long:** Writing – review & editing, Validation, Supervision, Resources, Project administration, Methodology, Funding acquisition, Conceptualization.

Declaration of Competing Interest

The authors declare that they have no known competing financial interests or personal relationships that could have appeared to influence the work reported in this paper.

Acknowledgement

Duong T. Nguyen acknowledged PhD scholarship support from the University of Technology Sydney. The authors also gratefully acknowledged financial support from the UTS – SHU Key Partnership Program and the UTS Global Strategic Partnership.

Appendix A. Supporting information

Supplementary data associated with this article can be found in the online version at doi:10.1016/j.jece.2025.119797.

Data availability

Data will be made available on request.

References

[1] T. Sidnell, R.J. Wood, J. Hurst, J. Lee, M.J. Bussemaker, Sonolysis of per- and poly fluoroalkyl substances (PFAS): a meta-analysis, Ultrason Sonochem. 87 (2022) 105944, https://doi.org/10.1016/j.ultsonch.2022.105944.
[2] J. Xiao, H. Li, J. Hu, Y. Wang, Y. Wang, Optimizing nanofiltration for PFOS removal: a gradient boosting convolutional model approach, J. Environ. Chem. Eng. 13 (4) (2025), https://doi.org/10.1016/j.jece.2025.117384.
[3] C. Gomri, D. Krzyzanowski, M. Rivallin, F. Zaviska, E. Petit, M. Semsarilar, M. Cretin, Electrochemical advanced oxidation of PFOA by Ti4O7 reactive electrochemical membrane anode, J. Environ. Chem. Eng. 12 (5) (2024), https://doi.org/10.1016/j.jece.2024.113495.
[4] F.L. Chiriac, C. Stoica, C. Iftode, F. Pirvu, V.A. Petre, I. Paun, L.F. Pascu, G. G. Vasile, M. Nita-Lazar, Bacterial biodegradation of perfluorooctanoic acid (PFOA) and perfluorosulfonic acid (PFOS) using pure pseudomonas strains, Sustainability 15 (18) (2023), https://doi.org/10.3390/su151814000.
[5] Z. Ilieva, R. Suehring, N. Bastos, F.-Z. Ezzahraoui, R. Hamza, Adsorption dynamics of four per-and polyfluoroalkyl substances (PFAS) onto activated sludge (AS) and aerobic granular sludge (AGS), J. Environ. Chem. Eng. 13 (3) (2025), https://doi.org/10.1016/j.jece.2025.116377.
[6] X. Lei, Q. Lian, X. Zhang, T.K. Karsili, W. Holmes, Y. Chen, M.E. Zappi, D.D. Gang, A review of PFAS adsorption from aqueous solutions: current approaches, engineering applications, challenges, and opportunities, Environ. Pollut. 321 (2023) 121138, https://doi.org/10.1016/j.envpol.2023.121138.
[7] M. Vakili, G. Cagnetta, S. Deng, W. Wang, Z. Gholami, F. Gholami, W. Dastyar, A. Mojiri, L. Blaney, Regeneration of exhausted adsorbents after PFAS adsorption: a critical review, J. Hazard Mater. 471 (2024) 134429, https://doi.org/10.1016/j.jhazmat.2024.134429.
[8] H. Abeysinghe, X. Ma, M. Tsige, PFAS removal via adsorption: a synergistic review on advances of experimental and computational approaches, Chemosphere 377 (2025) 144323, https://doi.org/10.1016/j.chemosphere.2025.144323.
[9] Y. Wang, S.B. Darling, J. Chen, Selectivity of Per- and polyfluoroalkyl substance sensors and sorbents in water, ACS Appl. Mater. Interfaces 13 (51) (2021) 60789–60814, https://doi.org/10.1021/acsami.1c16517.
[10] M. Afrooz, R. Zeynali, J. Soltan, K.N. McPhedran, A novel biochar adsorbent for treatment of perfluorooctanoic acid (PFOA) contaminated water: exploring batch and dynamic adsorption behavior, J. Water Process Eng. 69 (2025), https://doi.org/10.1016/j.jwpe.2024.106586.
[11] S.C.E. Leung, D. Wanninayake, D. Chen, N.T. Nguyen, Q. Li, Physicochemical properties and interactions of perfluoroalkyl substances (PFAS) - challenges and opportunities in sensing and remediation, Sci. Total Environ. 905 (2023) 166764, https://doi.org/10.1016/j.scitotenv.2023.166764.
[12] B. Teng, Z. Zhao, L. Xia, J. Wu, H. Wang, Progress on the removal of PFAS contamination in water by different forms of iron-modified biochar, Chemosphere 369 (2024) 143844, https://doi.org/10.1016/j.chemosphere.2024.143844.
[13] D. Liang, C. Li, H. Chen, E. Sormo, G. Cornelissen, Y. Gao, F. Reguyal, A. Sarmah, J. Ippolito, C. Kammann, F. Li, Y. Sailaukhanuly, H. Cai, Y. Hu, M. Wang, X. Li, X. Cui, B. Robinson, E. Khan, H. Wang, A critical review of biochar for the remediation of PFAS-contaminated soil and water, Sci. Total Environ. 951 (2024) 174962, https://doi.org/10.1016/j.scitotenv.2024.174962.
[14] A. Ghimire, G. Kumar, P. Sivagurunathan, S. Shobana, G.D. Saratale, H.W. Kim, V. Luongo, G. Esposito, R. Munoz, Bio-hythane production from microalgae biomass: key challenges and potential opportunities for algal bio-refineries, Bioresour. Technol. 241 (2017) 525–536, https://doi.org/10.1016/j.biortech.2017.05.156.
[15] D.T. Nguyen, M.A.H. Johir, T.M.I. Mahlia, A.S. Silitonga, X. Zhang, Q. Liu, L. D. Nghiem, Microalgae-derived biolubricants: challenges and opportunities, Sci. Total Environ. 954 (2024) 176759, https://doi.org/10.1016/j.scitotenv.2024.176759.
[16] A.A. Khan, J. Gul, S.R. Naqvi, I. Ali, W. Farooq, R. Liaqat, H. AlMohamadi, L. Stepanec, D. Juchelkova, Recent progress in microalgae-derived biochar for the treatment of textile industry wastewater, Chemosphere 306 (2022) 135565, https://doi.org/10.1016/j.chemosphere.2022.135565.
[17] X. Tian, S. Chu, Y. Hu, L. Luo, X. Lin, H. Wang, Removal of heavy metals from single- and multi-metal solution by magnetic microalgae-derived biochar, J. Water Process Eng. 69 (2025), https://doi.org/10.1016/j.jwpe.2024.106622.
[18] Z. Wang, A. Alinezhad, S. Nason, F. Xiao, J.J. Pignatello, Enhancement of per- and polyfluoroalkyl substances removal from water by pyrogenic carbons: tailoring carbon surface chemistry and pore properties, Water Res. 229 (2023), https://doi.org/10.1016/j.watres.2022.119467.
[19] B. Xu, S. Liu, J.L. Zhou, C. Zheng, J. Weifeng, B. Chen, T. Zhang, W. Qiu, PFAS and their substitutes in groundwater: occurrence, transformation and remediation, J. Hazard Mater. 412 (2021) 125159, https://doi.org/10.1016/j.jhazmat.2021.125159.
[20] Y.S. Ho, G. M, Pseudo-second order model for sorption processes, Process Biochem. 34 (1999) 451–465, https://doi.org/10.1016/S0032-9592(98)00112-5.
[21] Langmuir, The adsorption of gases on plane surfaces of glass, mica and platinum, J. Am. Chem. Soc. 40 (9) (1918) 1361–1403, https://doi.org/10.1021/ja02242a004.
[22] Freundlich, Uber die adsorption in losungen, Z. fur Phys. Chem. 57 (1906) 385–470.
[23] L. Ramirez Arenas, S. Ramseier Gentile, S. Zimmermann, S. Stoll, Nanoplastics adsorption and removal efficiency by granular activated carbon used in drinking water treatment process, Sci. Total Environ. 791 (2021) 148175, https://doi.org/10.1016/j.scitotenv.2021.148175.
[24] Z. Tan, S. Yuan, M. Hong, L. Zhang, Q. Huang, Mechanism of negative surface charge formation on biochar and its effect on the fixation of soil cd, J. Hazard Mater. 384 (2020) 121370, https://doi.org/10.1016/j.jhazmat.2019.121370.
[25] H. Li, Y. Cao, D. Zhang, B. Pan, pH-dependent K(OW) provides new insights in understanding the adsorption mechanism of ionizable organic chemicals on carbonaceous materials, Sci. Total Environ. 618 (2018) 269–275, https://doi.org/10.1016/j.scitotenv.2017.11.065.
[26] X.-F. Tan, S.-S. Zhu, R.-P. Wang, Y.-D. Chen, P.-L. Show, F.-F. Zhang, S.-H. Ho, Role of biochar surface characteristics in the adsorption of aromatic compounds: pore structure and functional groups, Chin. Chem. Lett. 32 (10) (2021) 2939–2946, https://doi.org/10.1016/j.cclet.2021.04.059.
[27] Y. Zhang, A. Thomas, O. Apul, A.K. Venkatesan, Coexisting ions and long-chain per- and polyfluoroalkyl substances (PFAS) inhibit the adsorption of short-chain PFAS by granular activated carbon, J. Hazard Mater. 460 (2023) 132378, https://doi.org/10.1016/j.jhazmat.2023.132378.
[28] N. Liu, C. Wu, G. Lyu, M. Li, Efficient adsorptive removal of short-chain perfluoroalkyl acids using reed straw-derived biochar (RESCA), Sci. Total Environ. 798 (2021) 149191, https://doi.org/10.1016/j.scitotenv.2021.149191.
[29] I.M. Militao, F. Roddick, L. Fan, L.C. Zepeda, R. Parthasarathy, R. Bergamasco, PFAS removal from water by adsorption with alginate-encapsulated plant albumin and rice straw-derived biochar, J. Water Process Eng. 53 (2023), https://doi.org/10.1016/j.jwpe.2023.103616.
[30] L. Ramirez Arenas, P. Le Coustumer, S. Ramseier Gentile, S. Zimmermann, S. Stoll, Removal efficiency and adsorption mechanisms of CeO(2) nanoparticles onto granular activated carbon used in drinking water treatment plants, Sci. Total Environ. 856 (Pt 2) (2023) 159261, https://doi.org/10.1016/j.scitotenv.2022.159261.
[31] A.K. Ilango, R. Mekkat, V. Jeyalakshmi, M.N. Pervez, T. Jiang, P. Chand, Y. Kumaran, H. Efstathiadis, D. Sukalingum, M. Soos, Y. Liang, Enhanced removal of PFAS in water using activated ZIF-8 carbons: high adsorption efficiency, repeatable regenerability and reusability, Chem. Eng. J. 507 (2025), https://doi.org/10.1016/j.cej.2025.160192.
[32] Q. Yu, R. Zhang, S. Deng, J. Huang, G. Yu, Sorption of perfluorooctane sulfonate and perfluorooctanoate on activated carbons and resin: kinetic and isotherm study, Water Res 43 (4) (2009) 1150–1158, https://doi.org/10.1016/j.watres.2008.12.001.
[33] H. Chen, S. Chen, X. Quan, Y. Zhao, H. Zhao, Sorption of perfluorooctane sulfonate (PFOS) on oil and oil-derived black carbon: influence of solution ph and [Ca2+, Chemosphere 77 (10) (2009) 1406–1411, https://doi.org/10.1016/j.chemosphere.2009.09.008.
[34] X. Chen, X. Xia, X. Wang, J. Qiao, H. Chen, A comparative study on sorption of perfluorooctane sulfonate (PFOS) by chars, ash and carbon nanotubes, Chemosphere 83 (10) (2011) 1313–1319, https://doi.org/10.1016/j.chemosphere.2011.04.018.
[35] X. Lei, L. Yao, Q. Lian, X. Zhang, T. Wang, W. Holmes, G. Ding, D.D. Gang, M. E. Zappi, Enhanced adsorption of perfluorooctanoate (PFOA) onto low oxygen content ordered mesoporous carbon (OMC): adsorption behaviors and mechanisms, J. Hazard Mater. 421 (2022) 126810, https://doi.org/10.1016/j.jhazmat.2021.126810.